

# Hardening of Thermal Photons Through Inverse Compton Scattering in Strong Magnetic Fields

Yi Xu and Hong-Hua Xu \*

Department of Physics, Shanghai Jiaotong University, Shanghai 200030

Received 2001 May 12; accepted 2001 June 4

**Abstract** A new spectrum function is obtained by use of the Compton scattering cross section in the laboratory frame derived earlier. This spectrum function, besides some modifications in the coefficients of the resonant term, contains also a non-resonant term which is inversely proportional to the square of the magnetic field. Based on this spectrum function, the hardening of thermal photons through inverse Compton scattering by relativistic electron beams on the surface of a strongly magnetized neutron star is investigated. Two new features are found. First, there is a maximum scattered photon energy for a given resonant scattering, beyond which resonance disappears. This maximum depends on the electron energy and the magnetic field, but is independent of the incident photon energy. Second, beyond each resonant scattering, there is a high-energy tail, resulting from non-resonant scattering. It is also found that all the tails have a common upper limit which is the highest scattered photon energy for the given incident photon and electron energies. These two new features are absent in the Monte Carlo simulations and therefore, may have physical implications for  $\gamma$ -ray emissions.

**Key words:** stars: neutron star — magnetic fields — scattering — gamma rays

## 1 INTRODUCTION

With the development of  $\gamma$ -ray burst astronomy, inverse Compton scattering in strong magnetic fields has attracted more and more attention and a great deal of work has been done on this subject (Daugherty & Harding 1989; Dermer 1990; Zhang & Qiao 1997; Harding & Muslimov 1998). Daugherty and Harding (1989) studied the  $\gamma$ -ray generation by Monte Carlo simulations based on Herold's cross section (Herold 1979) of magnetic Compton scattering in the electron rest frame (ERF). They calculated the Comptonized photon spectra at different heights above the surface of a neutron star, which is assumed to have a magnetic dipole field configuration. In the present paper we will give an analytical study of the  $\gamma$ -ray generation starting from the magnetic Compton scattering cross section in the laboratory frame (LF) which we derived earlier (Xu et al. 1998) and will give a calculation of the photon spectrum

---

\* E-mail: xuhh@mail.sjtu.edu.cn

resulting from the hardening of the thermal photons on the surface of a magnetized neutron star.

First, we recalculate the spectrum function of inverse magnetic Compton scattering given in our previous paper (Xu et al. 1998). By “spectrum function” we mean a function in terms of which the spectrum of the scattered photons can be calculated. Compared with our previous results, the recalculation modifies the coefficients in the resonance term and yields a new term inversely proportional to the square of the magnetic field. This new term is non-resonant and we call it hereafter the magnetic term. When the magnetic field is weak but is still within the range of pulsars, the magnetic term will affect the scattered spectrum significantly.

Then, with the help of the improved spectrum function we investigate the hardening of the thermal photons due to the Compton scattering by a beam of relativistic monochromatic electrons on the surface of a pulsar. Our new results, as will be shown in the text, consist of two parts. First, there is a maximum scattered photon energy for each resonant scattering, beyond which the resonance disappears. This maximum is closely related to the magnetic field: the stronger the magnetic field, the higher the maximum. Second, a high-energy tail occurs beyond each resonant scattering which is closely related to the magnetic term. It is found that all the tails have a common upper limit, the highest scattered photon energy for given incident photon and electron energies, which is independent of the magnetic field. This means that the highest scattered photon energy calculated from our spectrum function is higher than that from the Monte Carlo simulations (Daugherty & Harding 1989). These two new features may have physical implications for  $\gamma$ -ray emission and we hope they will be confirmed by observations.

## 2 CALCULATION OF THE SPECTRUM FUNCTION OF MAGNETIC INVERSE COMPTON SCATTERING

In order to recalculate the spectrum function of magnetic inverse Compton scattering, the full expression of the corresponding cross section in the LF is needed; this is quoted as follows (Xu et al. 1998):

$$\frac{d\sigma}{d\Omega_f} = \frac{r_0^2}{8} \frac{\Delta_f}{\Delta_{ir}(1+\gamma)(1+\gamma+\Delta_i-\Delta_f)} \times \frac{\exp\left[-\frac{B_c}{2B}\left(\Delta_f^2 \sin^2 \theta_f + \Delta_i^2 \sin^2 \theta_i\right)\right] |Y|^2}{\left[\gamma(1-\beta \cos \theta_f) + \Delta_i(1-\cos \theta_i \cos \theta_f) - \Delta_f \sin^2 \theta_f\right]}, \quad (1)$$

where  $B$  is the magnetic field with its direction taken to be along the  $z$ -axis,  $\Delta_i = \omega_i/m$ ,  $\Delta_f = \omega_f/m$  are the reduced incident and scattered photon energies ( $m$  is the electron rest energy),  $\theta_i$  and  $\theta_f$  are the incident and scattered photon angles with respect to the  $B$  field,  $\phi$ , the azimuth angle of the scattered photon (the azimuth angle of the incident photon is taken to be zero),  $\gamma$ , the electron energy,  $\beta = \sqrt{1-1/\gamma^2}$ ,  $r_0$ , the classical electron radius,  $B_c = \frac{m^2}{e} \approx 4.414 \times 10^9 T$  is the critical magnetic field, and  $\Delta_{ir}$ ,  $\Delta_{fr}$ ,  $\Delta_0$  are defined respectively by  $\Delta_{ir} = \gamma\Delta_i(1-\beta \cos \theta_i)$ ,  $\Delta_{fr} = \gamma\Delta_f(1-\beta \cos \theta_f)$ ,  $\Delta_0 = \frac{\omega_0}{m} = \frac{B}{B_c}$ , where  $\omega_0 = eB/m$  is the cyclotron energy.  $|Y|^2$  in Eq. (1) is given by

$$|Y|^2 = |Y(1_i \rightarrow 1_f)|^2 + |Y(1_i \rightarrow 2_f)|^2 + |Y(2_i \rightarrow 1_f)|^2 + |Y(2_i \rightarrow 2_f)|^2, \quad (2)$$

where  $\lambda_i \rightarrow \lambda_f$  represents the scattering of a photon from polarization  $\lambda_i$  to  $\lambda_f$ , and

$$\begin{aligned}
 Y(1_i \rightarrow 1_f) = & [(A_- \cos \theta_f - B_1) \cos \theta_i e^{i\phi} - B_2 \cos \theta_f e^{-i\phi}] \sum_{n=0}^{\infty} \zeta^n S_{i,n+1} e^{in\phi} \\
 & - [(A'_- \cos \theta_f + B_1) \cos \theta_i e^{-i\phi} + B_2 \cos \theta_f e^{i\phi}] \sum_{n=0}^{\infty} \zeta^n S_{f,n+1} e^{-in(\phi-\eta)} \\
 & + \sin \theta_i \sin \theta_f [A_+ \sum_{n=0}^{\infty} \zeta^n S_{i,n} e^{in\phi} - A_+ \sum_{n=0}^{\infty} \zeta^n S_{f,n} e^{-in(\phi-\eta)}], \tag{3}
 \end{aligned}$$

where

$$\left. \begin{aligned}
 A_{\pm} &= a \pm b(\beta\gamma - \Delta_f \cos \theta_f), \\
 A'_{\pm} &= a' \pm b(\beta\gamma - \Delta_f \cos \theta_f), \\
 B_1 &= b\Delta_f \sin^2 \theta_f, \\
 B_2 &= b\Delta_i \sin^2 \theta_i,
 \end{aligned} \right\} \tag{4}$$

in which

$$\left. \begin{aligned}
 a &= \beta\gamma(1 + \gamma + \Delta_i)(\beta\gamma + \Delta_i \cos \theta_i - \Delta_f \cos \theta_f) + (\gamma - 1 + \Delta_i)(1 + \gamma)(1 + \gamma + \Delta_i - \Delta_f), \\
 a' &= \beta\gamma(1 + \gamma - \Delta_f)(\beta\gamma + \Delta_i \cos \theta_i - \Delta_f \cos \theta_f) + (\gamma - 1 - \Delta_f)(1 + \gamma)(1 + \gamma + \Delta_i - \Delta_f), \\
 b &= \beta\gamma(1 + \gamma + \Delta_i - \Delta_f) + (\beta\gamma + \Delta_i \cos \theta_i - \Delta_f \cos \theta_f)(1 + \gamma),
 \end{aligned} \right\} \tag{5}$$

and

$$\left. \begin{aligned}
 \eta &= \zeta \sin \phi, \\
 \zeta &= \frac{B_c}{2B} \Delta_i \Delta_f \sin \theta_i \sin \theta_f, \\
 S_{i,n} &= \frac{1}{n! [2(\Delta_{ir} - n\Delta_0) + \Delta_i^2 \sin^2 \theta_i]}, \\
 S_{f,n} &= \frac{1}{n! [2(\Delta_{fr} + n\Delta_0) - \Delta_f^2 \sin^2 \theta_f]}.
 \end{aligned} \right\} \tag{6}$$

Other  $Y$ 's are given by

$$\begin{aligned}
 Y(1_i \rightarrow 2_f) = & i(A_- \cos \theta_i - B_2) \sum_{n=0}^{\infty} \zeta^n S_{i,n+1} e^{i(n+1)\phi} \\
 & + i(A'_- \cos \theta_i + B_2) \sum_{n=0}^{\infty} \zeta^n S_{f,n+1} e^{-i(n+1)\phi+i\eta}, \tag{7}
 \end{aligned}$$

$$\begin{aligned}
 Y(2_i \rightarrow 1_f) = & -i(A_- \cos \theta_f - B_1) \sum_{n=0}^{\infty} \zeta^n S_{i,n+1} e^{i(n+1)\phi} \\
 & -i(A'_- \cos \theta_f + B_1) \sum_{n=0}^{\infty} \zeta^n S_{f,n+1} e^{-i(n+1)\phi+i\eta}, \tag{8}
 \end{aligned}$$

$$Y(2_i \rightarrow 2_f) = A_- \sum_{n=0}^{\infty} \zeta^n S_{i,n+1} e^{i(n+1)\phi} - A'_- \sum_{n=0}^{\infty} \zeta^n S_{f,n+1} e^{-i(n+1)\phi + i\eta}. \quad (9)$$

In astrophysics one is more interested in the inverse Compton scattering of a low energy photon by a relativistic electron in strong magnetic fields satisfying  $\Delta_i \ll 1$ ,  $\gamma \gg 1$ . We consider first the condition  $\Delta_i \ll 1$ . In this case the summations in Eqs. (7)–(9) converge rapidly, so that keeping only the term  $n = 0$  is already a satisfactory approximation. To show this we first integrate over the azimuth angle  $\phi$  and retain only the leading terms, then the differential cross section (1) is reduced to

$$d\sigma = \sigma(\Delta_i, \theta_i, \gamma, \theta_f) \sin \theta_f d\theta_f, \quad (10)$$

where

$$\sigma(\Delta_i, \theta_i, \gamma, \theta_f) = \frac{\pi r_0^2}{4} \frac{\Delta_f}{\Delta_{ir}(\gamma+1)(1+\gamma+\Delta_i-\Delta_f)} \frac{\exp\left(-\frac{B_c}{2B} \Delta_f^2 \sin^2 \theta_f\right) Y_r}{\left[\gamma(1-\beta \cos \theta_f) + \Delta_i(1-\cos \theta_i \cos \theta_f) - \Delta_f \sin^2 \theta_f\right]}, \quad (11)$$

and  $Y_r$  is given by

$$Y_r = C_1 S_{i,1}^2 + C_2 S_{f,1}^2 + \left[ (A_+ S_{i,0} - A'_+ S_{f,0})^2 + 2(1 - J_0(\zeta)) A_+ A'_+ S_{i,0} S_{f,0} \right] (\sin \theta_i \sin \theta_f)^2, \quad (12)$$

in which

$$C_1 = (A_- \cos \theta_f - B_1)^2 (1 + \cos^2 \theta_i) + (A_- \cos \theta_i - B_2)^2 + (B_2 \cos \theta_f)^2 + A_-^2, \quad (13)$$

$$C_2 = (A'_- \cos \theta_f + B_1)^2 (1 + \cos^2 \theta_i) + (A'_- \cos \theta_i + B_2)^2 + (B_2 \cos \theta_f)^2 + A_-^2, \quad (14)$$

and  $J_0(\zeta)$  is the zeroth order Bessel function. It is worth pointing out here that the approximation (12) can also be justified by considering the nonrelativistic limit in the ERF ( $\gamma = 1$  or  $\beta = 0$ ). In fact, under the Thomson limit ( $\Delta_f \approx \Delta_i \ll 1$ ) it is easy to see that  $J_0(\zeta) \approx 1$ ,  $A_- = -A'_- \approx 4\Delta_i$ ,  $B_1 = B_2 \approx 0$  and  $A_+ = -A'_+ \approx 4\Delta_i$ , then Eq.(11) can be simplified to

$$\frac{\sigma(\Delta_i, \theta_i, \theta_f)}{\pi r_0^2} = \sin^2 \theta_i \sin^2 \theta_f + \frac{1}{4} (1 + \cos^2 \theta_i) (1 + \cos^2 \theta_f) \left[ \frac{\Delta_i^2}{(\Delta_i - \Delta_0)^2} + \frac{\Delta_i^2}{(\Delta_i + \Delta_0)^2} \right], \quad (15)$$

which is just Herold's nonrelativistic result, a well known widely used expression. However, Eq.(11) together with Eq. (12) is also valid for the relativistic case.

In the following we use this simplified cross section to calculate the spectrum function of the magnetic inverse Compton scattering. In the present paper, we concentrate our attention on the scattering by a monochromatic ( $\gamma$ ) electron beam. The density of scattered photons per unit time is

$$\frac{dN(\gamma)}{dt} = n_e \int \sin \theta_i d\theta_i \int \sin \theta_f d\theta_f \int n(\Delta_i) d\Delta_i (1 - \beta \cos \theta_i) \sigma(\Delta_i, \theta_i, \gamma, \theta_f) f(\cos \vartheta_i), \quad (16)$$

where  $n_e$  is the density of the electron beam and  $f(\cos\vartheta_i)$  an anisotropic factor for the incident photons. If the incident photons are isotropic, then  $f(\cos\vartheta_i) = 1$ . Taking into account energy conservation and the condition  $\Delta_i \ll 1$ , it is easy to derive

$$\sin\theta_f d\theta_f = -\frac{\gamma(1 - \beta \cos\theta_f) + \Delta_i(1 - \cos\theta_i \cos\theta_f) - \Delta_f \sin^2\theta_f}{\Delta_f(\gamma - \Delta_f \cos\theta_f)} d\Delta_f. \quad (17)$$

With substitution of this variable transformation in Eq.(16), the spectrum of power density per unit scattered photon energy of a low frequency photon gas scattered by the monochromatic electron beam can be derived:

$$\frac{\Delta_f dN(\gamma, \Delta_f)}{dt d\Delta_f} = 8\pi r_0^2 n_e \int n(\Delta_i) d\Delta_i F(\gamma, \Delta_i, \Delta_f), \quad (18)$$

where

$$F(\gamma, \Delta_i, \Delta_f) = \int \sin\theta_i d\theta_i \frac{\Delta_f}{\Delta_i} \frac{Y_r \exp\left[-\frac{B_c}{2B} \Delta_f^2 \sin^2\theta_f\right]}{32\gamma^2(\gamma - \Delta_f)(\gamma - \Delta_f \cos\theta_f)} f(\cos\vartheta_i), \quad (19)$$

is just the desired spectrum function. Now we take into account the condition  $\gamma \gg 1$ , and then it is easy to show

$$\left. \begin{aligned} A_- &= [2\gamma - \Delta_f(1 + \cos\theta_f)] \Delta_{ir}, \\ A'_- &= -[2\gamma - \Delta_f(1 + \cos\theta_f)] \Delta_{fr}, \\ A_+ &= [2\gamma - \Delta_f(1 + \cos\theta_f)] 2\gamma^2, \\ A'_+ &= [2\gamma - \Delta_f(1 + \cos\theta_f)] (2\gamma^2 - \Delta_{fr}), \\ B_1 &= [2\gamma - \Delta_f(1 + \cos\theta_f)] (1 + \cos\theta_f) \Delta_{fr}, \\ B_2 &= [2\gamma - \Delta_f(1 + \cos\theta_f)] (1 + \cos\theta_i) \Delta_{ir}, \end{aligned} \right\} \quad (20)$$

and the spectrum function can be simplified accordingly to

$$F(\gamma, \Delta_i, \Delta_f) = \int \sin\theta_i d\theta_i \frac{\Delta_f}{\Delta_i} \frac{Y'_r}{32\gamma^2} \exp\left[-\frac{B_c}{2B} \Delta_f^2 \sin^2\theta_f\right] f(\cos\vartheta_i), \quad (21)$$

where

$$\begin{aligned} Y'_r &= \frac{D_1}{(\Delta_{ir} - \Delta_0)^2 + \Gamma_0^2} + \frac{D_2}{\left(\Delta_{fr} + \Delta_0 - 0.5\Delta_f^2 \sin^2\theta_f\right)^2} \\ &+ \left[ \frac{2\gamma^2}{\Delta_{ir}} - \frac{2\gamma^2 - \Delta_{fr}}{\Delta_{fr} - 0.5\Delta_f^2 \sin^2\theta_f} \right]^2 \sin^2\theta_i \sin^2\theta_f \\ &+ \frac{4[1 - J_0(\zeta)]\gamma^2(2\gamma^2 - \Delta_{fr})\sin^2\theta_i \sin^2\theta_f}{\Delta_{ir}(\Delta_{fr} - 0.5\Delta_f^2 \sin^2\theta_f)}, \end{aligned} \quad (22)$$

in which

$$\left. \begin{aligned} D_1 &= [\Delta_{ir} \cos\theta_f - \Delta_{fr}(1 + \cos\theta_f)]^2 (1 + \cos^2\theta_i) + \Delta_{ir}^2 [2 + (1 + \cos\theta_i)^2 \cos^2\theta_f], \\ D_2 &= [\Delta_{ir}(1 + \cos\theta_i) - \Delta_{fr} \cos\theta_i]^2 + \Delta_{fr}^2 (2 + \cos^2\theta_i) + \Delta_{ir}^2 (1 + \cos\theta_i)^2 \cos^2\theta_f, \end{aligned} \right\} \quad (23)$$

and  $\Gamma_0$  is related to the inverse life time of an electron in intermediate states which is usually estimated according to the transition rate of an electron from the first Landau level to the ground state (Daugherty & Vantura 1978), that is,  $\Gamma_0 = \frac{2}{3}\alpha (B/B_c)^2$  with  $\alpha$  the fine structure constant. In obtaining Eq.(21), use has been made of the following approximation

$$\frac{[2\gamma - \Delta_f (1 + \cos \theta_f)]^2}{4(\gamma - \Delta_f)(\gamma - \Delta_f \cos \theta_f)} \approx 1. \quad (24)$$

To see this we note that  $\Delta_f$  reaches maximum only at  $\theta_f = 0$  and  $\theta_i = \pi$ , so  $\Delta_f \ll \gamma$  if  $\theta_f$  is not close to zero and then Eq. (24) holds; if  $\theta_f$  is close to zero, then it is clear that Eq. (24) is also valid, thus the approximation is justified. It can be shown that  $\Delta_f \sin \theta_f$  can also be neglected if there are other dominant terms. Using again the energy conservation, we get the following approximate expression,

$$\left[1 - \beta \cos \theta_f + \frac{\Delta_i}{\gamma} (1 - \cos \theta_i \cos \theta_f)\right] \Delta_f = (1 - \beta \cos \theta_i) \Delta_i. \quad (25)$$

For further simplification, we consider the case where  $\theta_f$  is not close to zero, then Eq. (25) can be simplified to

$$(1 - \beta \cos \theta_f) \Delta_f = (1 - \beta \cos \theta_i) \Delta_i. \quad (26)$$

This means that the Doppler frequencies of the incident and scattered photons are equal,  $\Delta_{ir} = \Delta_{fr}$ , which is just the Thomson limit in the LF. Equation (25) tells us also that the highest scattered photon energy is of magnitude  $(1 + \beta)^2 \gamma^2 \omega_i / (1 + 2(1 + \beta) \gamma \Delta_i) \approx 4\gamma^2 \omega_i / (1 + 4\gamma \Delta_i)$ , which becomes  $4\gamma^2 \omega_i$  for  $\gamma \Delta_i \ll 1$ . This is a well-known feature of inverse Compton scattering. Applying the Thomson limit Eq. (26) and expanding  $J_0(\zeta)$  up to  $\zeta^2$ , Eq. (22) is reduced to

$$Y'_r = \frac{C \Delta_{ir}^2}{(\Delta_{ir} - \Delta_0)^2 + \Gamma^2} + \frac{C \Delta_{ir}^2}{(\Delta_{ir} + \Delta_0)^2} + (\sin \theta_i \sin \theta_f)^2 + 0.5 [\Delta_{ir} (1 + \cos \theta_i) (1 + \cos \theta_f) B_c/B]^2, \quad (27)$$

where the coefficient  $C$  is defined by

$$C = (1 + \cos^2 \theta_i) (1 + \cos^2 \theta_f) + 2 (1 + \cos \theta_i \cos^2 \theta_f). \quad (28)$$

Setting  $x = (1 - \cos \theta_i) \approx (1 - \beta \cos \theta_i)$ , with its lower limit being determined by Eq. (25)

$$x_{\min} \approx \frac{\Delta_f}{2\gamma^2 \Delta_i (1 - \Delta_f/\gamma)}, \quad (29)$$

the spectrum function can be expressed as

$$F = F_1 + F_2 + F_3, \quad (30)$$

in which

$$F_1 = \frac{\omega_r}{32\gamma^2} \int_{x_{\min}}^2 dx \left[ \frac{x^2 c(x)}{(x - a_0)^2 + \Gamma_0^2} + \frac{x^2 c(x)}{(x + a_0)^2} \right] f(1 - x), \quad (31)$$

$$F_2 = \frac{1}{32\gamma^2} \int_{x_{\min}}^2 dx (2-x) \left(2 - \frac{x}{\omega_r}\right) x^2 f(1-x), \quad (32)$$

$$F_3 = \frac{\omega_r \Delta_i^2}{64} \left(\frac{B_c}{B}\right) \int_{x_{\min}}^2 dx \left[x(2-x) \left(2 - \frac{x}{\omega_r}\right)\right]^2 f(1-x), \quad (33)$$

where,  $\omega_r = \frac{\omega_f}{\omega_i}$ ,  $a_0 = \frac{\omega_0}{\gamma\omega_i}$ ,  $\Gamma = 2\alpha(B/B_c)^2/3\gamma^2\Delta_i$ , and  $c(x)$  can be read from Eq. (28),

$$c(x) = (2 - 2x + x^2) \left(2 - \frac{2x}{\omega_r} + \frac{x^2}{\omega_r^2}\right) + 2 \left[1 + (1-x) \left(1 - \frac{x}{\omega_r}\right)^2\right]. \quad (34)$$

A simple investigation will show that  $F_2$  is much smaller than  $F_1$  or  $F_3$ . So the dominant contribution to the spectrum function is from  $F_1$  and  $F_3$ . Resonant scattering occurs when  $x_{\min} \leq a_0 \leq 2$  is satisfied where  $F_1$  becomes very large. This means that resonant scattering becomes operative when the following conditions are satisfied:

$$\frac{\omega_0}{\gamma\omega_i} \leq 2 \quad \text{and} \quad \frac{\omega_0}{\gamma\omega_i} \geq \frac{\omega_f}{2\gamma^2\omega_i(1 - \Delta_f/\gamma)},$$

which can be expressed alternatively by

$$\omega_i \geq \frac{\omega_0}{2\gamma} \quad \text{and} \quad \omega_f \leq \frac{2\gamma\omega_0}{1 + 2\Delta_0}. \quad (35)$$

For simplicity only, we consider, from this point on, the isotropic case, i.e.,  $f(1-x) = 1$ . Then the spectrum function can be plotted for different magnetic field strengths as in Fig. 1, where  $\varepsilon$  is the reduced energy of scattered photons,  $\varepsilon = \omega_f/4\gamma^2\omega_i$ . This figure shows that the efficiency of resonant scattering (for small  $B$  fields) is much higher than that of non-resonant scattering (for large  $B$  fields). We should point out here that the contribution of  $F_3$  is usually smaller than  $F_1$ , even for the non-resonant scattering. However when  $a_0 < x_{\min}$ , i.e.,  $\omega_f > \frac{2\gamma\omega_0}{1+2\Delta_0}$ ,  $F_3$  will play an important role in the non-resonant scattering (see Fig. 4). It is seen from Eq. (35) that the maximum energy of scattered photon resulting from the magnetic resonant scattering is given by

$$\omega_{\text{res}} = \frac{2\gamma\omega_0}{1 + 2\Delta_0}, \quad (36)$$

which depends on the incident electron energy and the magnetic field, but is independent of the incident photon energy.

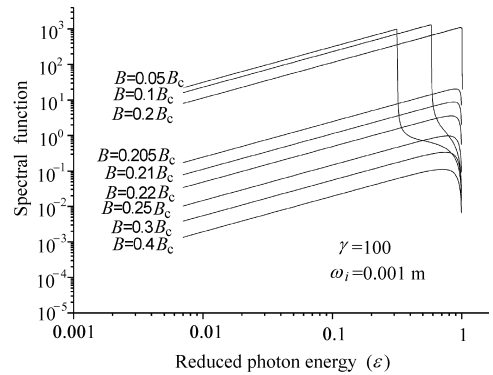


Fig. 1 Spectral function of the magnetic inverse Compton scattering. The scattered photon energy is a reduced one ( $\varepsilon = \omega_f/4\gamma^2\omega_i$ ). It is seen that the weaker is the  $B$  field, the larger is the function value (i.e., the higher is the scattering efficiency).

### 3 INVERSE COMPTON SCATTERING OF THERMAL PHOTONS ON THE SURFACE OF A PULSAR

Due to the high temperature near the cap of a pulsar,  $T \sim 10^6$  K, there is a large number of soft X-ray photons resulting from thermal radiation. On the other hand, there are also high-energy electron beams in the magnetosphere produced by electrostatic acceleration. According to Eq. (35), these two conditions make it possible to produce hard X-ray and  $\gamma$ -ray emissions on the surface of a strongly magnetized pulsar through the resonant magnetic Compton scattering.

The spectrum of black body radiation is

$$n(\omega_i) d\omega_i = \frac{1}{\pi^2} \frac{\omega_i^2}{e^{\frac{\omega_i}{kT}} - 1} d\omega_i. \quad (37)$$

Then the power density of scattered photons per unit scattered photon energy can be expressed as

$$\frac{dP(\omega_f)}{d\omega_f} = 8\pi r_0^2 n_e \int n(\omega_i) d\omega_i F(\gamma, \omega_i, \omega_f). \quad (38)$$

Alternatively, the scattered photon density per unit scattered photon energy and per unit time is

$$\frac{dN(\omega_f)}{d\omega_f dt} = 8\pi r_0^2 n_e \int n(\omega_i) d\omega_i F(\gamma, \omega_i, \omega_f) / \omega_f. \quad (39)$$

In the actual calculations, we assume  $T = 10^6$  K and  $\gamma = 100$  which are typical values for pulsars. Besides, for simplicity but without loss of generality, we set  $n_e = 1$ . Due to the resonant scattering condition  $\omega_i \geq \omega_0/2\gamma$ , only a small portion of thermal photons in Eq. (37) contribute to the resonant scattering if the magnetic field is very strong. A simple estimation shows that the non-resonant scattering is dominant if  $B > 0.3B_c$ . On the other hand, if the magnetic field is relatively weak,  $B < 0.3B_c$ , then the resonant scattering is dominant.

We consider first the power spectrum of scattered photons. Figures 2a, 2b, and 2c are plotted according to Eq. (38) for different values of the magnetic field strength. Figures 2a and 2b assume that, far away from the resonant region ( $B \geq 0.5B_c$ ), soft X-ray photons are hardened to  $\gamma$ -ray photons mainly through the non-resonant scattering and the shape of the spectrum is similar to that of a black body. In Fig. 2c the magnetic field is relatively weak ( $B = 0.34B_c$ ) and resonant scattering begins to act, the power spectrum of scattered photon differs remarkably from that of the black body radiation, i.e., the distribution of scattered photons is shifted to the high-energy end due to the increase of the scattering efficiency. This fact indicates that the strength of magnetic field plays an important role in the magnetic inverse Compton scattering.

Next we consider the spectrum of the scattered photon number for the non-resonant case. Following Daugherty and Harding (1989), the magnetic field near the pole on the surface of the neutron star is assumed to have a dipole configuration  $B = B_0 [r_0 / (r_0 + z)]^3$  where  $r_0$  is the radius of the star and  $z$  is the height above the star and  $B_0 = 1.14B_c$ . Based on Eq. (39) the rate of scattered photon density is calculated from  $z = 0.05r_0$  up to  $z = 0.5r_0$  with a step  $\Delta z = 0.05r_0$  and the results are shown in Fig. 3. It shows that, as the magnetic field becomes weaker, the rate of production of high-energy photons goes up. This means that the energy-loss of electrons in the process of magnetic Compton scattering increases as the magnetic field strength decreases. It is worth pointing out here that all three figures have a common upper limit for the scattered photon energy,  $\omega_{f \max} = 4\gamma^2 \omega_i / (1 + 4\gamma \Delta_i)$ , which is the highest photon energy in the nonmagnetic Compton scattering.

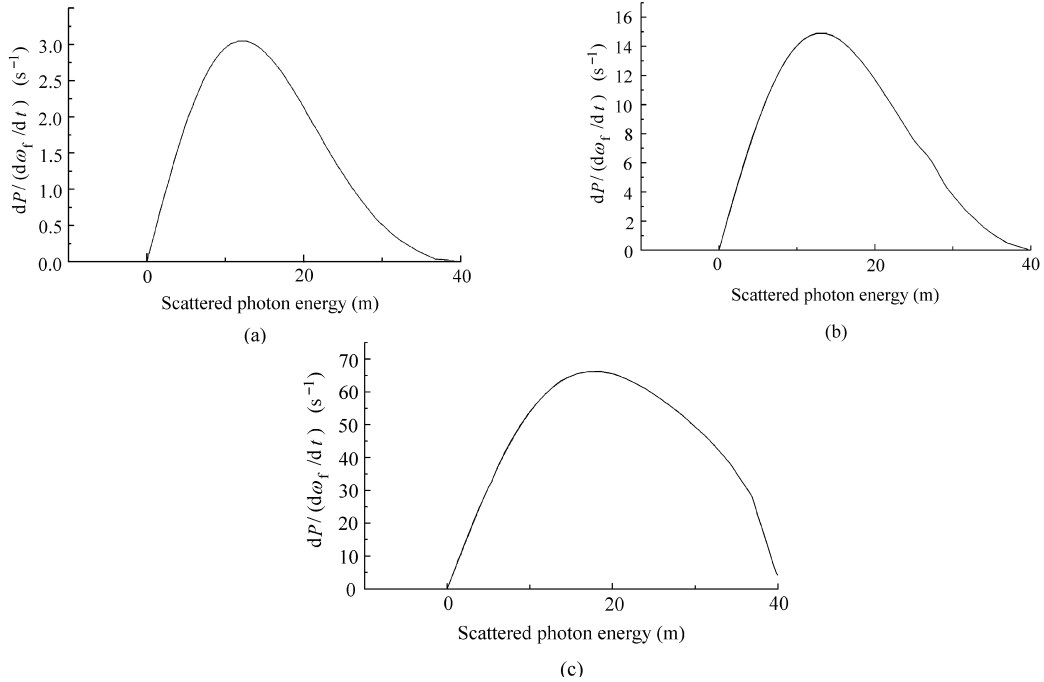


Fig. 2 The power density spectra due to Comptonization of thermal photons by monoenergetic injected electrons at  $\gamma = 100$  for  $T = 10^6$  K and different  $B$  fields. The spectra in Figs. 2a and 2b with  $B = 0.5 B_c$  have a shape similar to that of the black body radiation. While Fig. 2c with  $B = 0.34 B_c$  differs from black body radiation due to the shift of distribution of photons to the high-energy end.

Now we check the rate of scattered photon density for the resonant case. Results of numerical calculations are shown in Fig. 4, for the magnetic field strength  $B_0 = 0.2B_c$ . This figure differs considerably from corresponding figure (figure 9) in Daugherty and Harding's paper. First, each resonant scattering has its own maximum  $\omega_{\text{res}}$  (depending on  $B$ ), beyond which the scattered photon number decreases sharply and the high-energy tail begins. While in fig. 9 in Daugherty and Harding's paper every resonant scattering terminates at a common point (independent of  $B$ ) which seems to be the highest scattered photon energy, and there are no high-energy tails. In fact the high-energy tails in Fig. 4 result from the non-resonant Compton scattering, which is closely related to the magnetic term as mentioned at the end of Section 2, the weaker the magnetic field is, the more important the magnetic term and the longer the tail will be. Also, the highest scattered photon energy  $\omega_{f \text{ max}}$ , the same in Figs. 1–3, is much higher than that obtained by Daugherty and Harding (1989). Though the photon production rate in the high-energy tail is much smaller than in the resonant part, it indicates that the magnetic inverse Compton scattering can yield a much higher photon energy than that obtained by Daugherty and Harding. However it might be that only few photons with energies higher than the threshold could escape due to the production of electron-positron pairs through several channels, for example, through the collision of a high-energy photon with a low-energy one (Lightman & Zdziarski 1987), or the production by single photons in strong magnetic fields (Daugherty & Harding 1987).

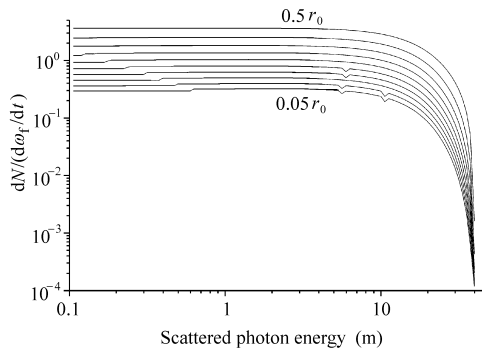


Fig. 3 The spectra of the rate of scattered photon density per scattered photon energy, assuming monoenergetic injected electrons at  $\gamma = 100$  for  $B_0 = 1.14 B_c$  and  $T = 10^6$  K. Spectra are plotted from  $0.05 r_0$  up to  $0.5 r_0$  with  $\Delta z = 0.05 r_0$ .

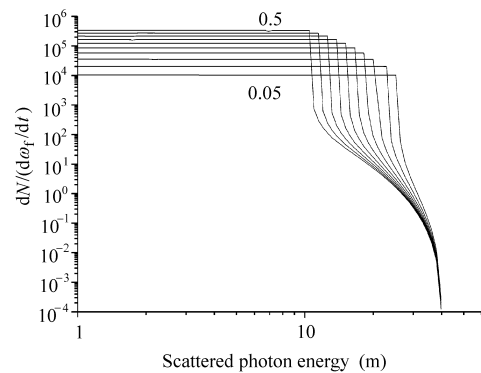


Fig. 4 The spectra of the rate of scattered photon density per unit scattered photon energy, assuming monoenergetic injected electrons at  $\gamma = 100$  for  $B = 0.2 B_c$  and  $T = 10^6$  K. Spectra are plotted from  $0.05 r_0$  up to  $0.5 r_0$  with a step  $\Delta z = 0.05 r_0$ . The flat part comes from the resonant scattering and the high-energy tails result from the non-resonant scattering which is closely related to the magnetic term.

To conclude, we have recalculated the spectrum function of magnetic inverse Compton scattering in the laboratory frame. A new term, the magnetic term, is obtained which is absent in the previous work. With help of this new spectrum function the Comptonization of thermal photons at the surface of a magnetized neutron star is investigated. Compared with previous numerical simulations (Daugherty & Harding 1989), our calculated spectrum for scattered photons shows that every resonant scattering has its own field-depending terminate point beyond which there is a high-energy tail which is closely related to the magnetic term. It is shown also that all the high-energy tails have a common terminating point, the highest scattered photon energy, which is much higher than that obtained by above mentioned numerical simulations.

## References

- Daugherty J. K., Vantura J., 1978, Phys. Rev., D18, 1053  
 Herold H., 1979, Physics. Rev., D19, 2868  
 Lightman A. P., Zdziarski A. A., 1987, ApJ, 319, 643  
 Daugherty J. K., Harding A. K., 1987, ApJ, 273, 761  
 Daugherty J. K., Harding A. K., 1989, ApJ, 336, 861  
 Dermer C. D., 1990, ApJ, 360, 197  
 Preece R. D., Harding A. K., 1992, ApJ, 386, 308  
 Zhang B., Qiao G. J., 1997, ApJ, 478, 313  
 Xu Honghua et al., 1998, Science in China (Series A), 41, 1184